Journal of Geodesy (2019) 93:45–64
https://doi.org/10.1007/s00190-018-1138-y

ORIGINAL ARTICLE

Improving multi-GNSS ultra-rapid orbit determination for real-time precise point positioning

Xingxing Li[1] · Xinghan Chen[1] · Maorong Ge[1] · Harald Schuh[1]

Received: 4 August 2017 / Accepted: 18 March 2018 / Published online: 27 March 2018

Abstract
Currently, with the rapid development of multi-constellation Global Navigation Satellite Systems (GNSS), the real-time positioning and navigation are undergoing dramatic changes with potential for a better performance. To provide more precise and reliable ultra-rapid orbits is critical for multi-GNSS real-time positioning, especially for the three merging constellations Beidou, Galileo and QZSS which are still under construction. In this contribution, we present a five-system precise orbit determination (POD) strategy to fully exploit the GPS + GLONASS + BDS + Galileo + QZSS observations from CDDIS + IGN + BKG archives for the realization of hourly five-constellation ultra-rapid orbit update. After adopting the optimized 2-day POD solution (updated every hour), the predicted orbit accuracy can be obviously improved for all the five satellite systems in comparison to the conventional 1-day POD solution (updated every 3 h). The orbit accuracy for the BDS IGSO satellites can be improved by about 80, 45 and 50% in the radial, cross and along directions, respectively, while the corresponding accuracy improvement for the BDS MEO satellites reaches about 50, 20 and 50% in the three directions, respectively. Furthermore, the multi-GNSS real-time precise point positioning (PPP) ambiguity resolution has been performed by using the improved precise satellite orbits. Numerous results indicate that combined GPS + BDS + GLONASS + Galileo (GCRE) kinematic PPP ambiguity resolution (AR) solutions can achieve the shortest time to first fix (TTFF) and highest positioning accuracy in all coordinate components. With the addition of the BDS, GLONASS and Galileo observations to the GPS-only processing, the GCRE PPP AR solution achieves the shortest average TTFF of 11 min with 7° cutoff elevation, while the TTFF of GPS-only, GR, GE and GC PPP AR solution is 28, 15, 20 and 17 min, respectively. As the cutoff elevation increases, the reliability and accuracy of GPS-only PPP AR solutions decrease dramatically, but there is no evident decrease for the accuracy of GCRE fixed solutions which can still achieve an accuracy of a few centimeters in the east and north components.

Keywords Multi-GNSS · Hourly ultra-rapid orbit · Precise orbit determination · Real-time PPP · Precise point positioning

1 Introduction

Over the past decade, apart from the ongoing modernization of the GPS and GLONASS, the three new and emerging navigation satellite systems, i.e., BDS, Galileo and Quasi-Zenith Satellite System (QZSS), have already been offering a space-based position, navigation and timing (PNT) service. This will bring great opportunities and challenges for more precise and reliable GNSS applications (Prange et al. 2017). Since October 2011, the Russian GLONASS constellation has been fully recovered and currently is operating at full capability with 24 satellites in orbits and enabling full global coverage (Cai and Gao 2013; Wang et al. 2015). At present, Galileo is in the transition phase to full operational capability (FOC) and started offering initial operational capability (IOC) on December 15, 2016. As of December 2016, the Galileo system has 18 satellites in orbit, not all of which are really operable. By late 2018, the Galileo constellation is expected to consist of 26 available satellites in the Medium Earth Orbit (MEO) planes. Concerning QZSS, one geostationary satellite and two additional satellites are scheduled to be launched in 2017. The BDS navigation satellite system, which is in the phase of being established independently by China, is pacing steadily forward toward its final destination—an operational global navigation satellite system with a constellation of 5 Geostationary Earth Orbit (GEO), 3 Inclined GeoSynchronous Orbit (IGSO), and 27 MEO satellites by 2020.

✉ Xinghan Chen
xchen@gfz-potsdam.de

[1] German Research Centre for Geosciences (GFZ), Telegrafenberg, 14473 Potsdam, Germany

The second generation of the BDS system, known as BDS-2, has been offering PNT services to users in the Asia–Pacific region since December 2012 (Shi et al. 2013; Montenbruck et al. 2013). In 2015, China started the buildup of the third generation BDS system (BDS-3) for global coverage. The first BDS-3 satellite was launched on September 30, 2015. As of March 2016, there are four in-orbit validation BDS-3 satellites operable. The BDS-3 satellites transmit several new signals, i.e., B1C (1575.42 MHz), B2a (1176.45 MHz) and B2b (1207.14 MHz). It has been demonstrated that the observation quality of the new BDS-3 signals is comparable to that of GPS L1/L2/L5 and Galileo E1/E5a/E5b signals and the elevation-dependent code biases previously identified to exist in the code observations from the BDS-2 satellites are not notable for the new signals of the BDS-3 satellites (Zhang et al. 2017). With the increase in the number of available satellites, the fusion of multiple GNSS constellations will not only enhance PNT applications, but also provide an increased number of signals for space weather applications that employs the ray tracing of the neutral atmosphere and the ionosphere and the occultation techniques (Jakowski et al. 2005).

The International GNSS Service (IGS), as important component of Global Geodetic Observing System (GGOS), is fully committed for providing the highest-quality GNSS data, products and services in support of scientific and engineering applications. The MGEX pilot project has been initiated by the IGS to collect and analyze GNSS signals, and the MGEX analysis centers are responsible for assessing new satellite signals, comparing equipment performance and further developing the software to process multi-GNSS data and generate the related products. As a backbone of the MGEX project, over the past 5 years, a new network of multi-GNSS tracking stations has been established all over the world in parallel to the legacy IGS network for GPS and GLONASS. The MGEX network rapidly grew to about 170 active stations in October 2016. Leading supporters comprise Deutsches GeoForschungsZentrum (GFZ), Institut National de l'Information Géographique et Forestière (IGN), Bundesamt für Kartographie und Geodäsie (BKG), Geoscience Australia (GA), the Centre National d'Etudes Spatiales (CNES), Japan Aerospace Exploration Agency (JAXA), Deutsches Zentrum für Luft- und Raumfahrt (DLR) and the European Space Agency (ESA), which contribute almost three quarters of the multi-GNSS tracking stations (Montenbruck et al. 2017). Since the buildup of the multi-GNSS experiment, data collected by the MGEX stations have been archived by the three IGS data centers of IGN, BKG and the Crustal Dynamics Data Information System (CDDIS). Besides the archived RINEX data, roughly half of all IGS GNSS tracking stations also provide real-time data streams, which are disseminated based on a dedicated BKG caster (http://mgex.igs-ip.net). This is an important prerequisite for the multi-GNSS real-time precise clock estimation (PCE). Recently, most of the multi-GNSS real-time studies and MGEX ultra-rapid products focus on single-system or dual-system (e.g., GPS/GLONASS, GPS/BDS, GPS/Galileo) modes (Li et al. 2013; Teunissen et al. 2014; Geng and Shi 2017). Hadas and Bosy used a method of short-term prediction of real-time service (RTS) corrections that extend the application period of obsolete correction data without a significant loss in orbit quality (Hadas and Bosy 2015). Li et al. (2015) presented a GPS + GLONASS + BDS + Galileo four-system model for a prototype multi-GNSS float PPP system and demonstrated the feasibility of POD, PCE and PPP in simulated real-time mode. El-Mowafy et al. (2017) offered a method to maintain real-time PPP with 3D accuracy less than 10 cm when a discontinuity in receiving the orbit and clock corrections over a period from several minutes to hours occurred.

In this contribution, we fully exploit all the five navigation satellite systems (i.e., GPS + GLONASS + BDS + Galileo + QZSS) and implement an efficient multi-GNSS hourly POD processing for precise point positioning ambiguity resolution. An improved POD strategy is proposed to promote the real-time orbit accuracy and computational efficiency for generating the multi-GNSS hourly ultra-rapid orbit products. Our results also show that the orbit products derived from the proposed POD strategy can improve the real-time clock estimates. Based on the real-time orbits and clocks, we analyze the contribution of multi-GNSS to real-time PPP AR. The article is organized as follows. We first present an overview of the current status of the multi-GNSS constellations and available multi-GNSS real-time tracking networks including the MGEX network and IGS networks in Sect. 2. Afterward the multi-GNSS observational model and optimizing processing strategies for multi-GNSS hourly POD are introduced in Sect. 3. In Sect. 4, the comparative analyses concerning the improving POD strategy are given. Additionally, we evaluate the real-time orbit quality as well as the performance of multi-GNSS PPP AR in Sect. 4. The summary and conclusions are presented in Sect. 5.

2 Multi-GNSS constellations and tracking networks

2.1 Current status of the multi-GNSS constellations

Currently, the U.S. Global Positioning System (GPS) constellation is made up of 31 operational satellites. After launching an adequate number of GPS III satellites, it is expected that 24 operational satellites with the capability of broadcasting the L2C signal will be available by 2018 and twenty-four satellites broadcasting the L5 signal are appraised to be in orbit in 2024. All the Block IIA satellites that have served

as the backbone of GPS for about 2 decades, were finally decommissioned in early 2016. However, they are required to be kept in orbit in case there is a need to reactive them. In the GLONASS constellation, there are 23 operational GLONASS-M satellites, as well as both one GLONASS-M+ and one GLONASS-K1 satellites supporting transmission of the new L3 signal. Next to the ongoing modernization of U.S. GPS and Russia's GLONASS, the European Galileo system has presently launched 18 satellites, including the 4 IOV (three operational and one unavailable) and 12 FOC operational satellites, and two FOC satellites in the commissioning phase. The QZSS system, as a regional satellite-based augmentation system for GPS, is planned to operate three IGSO satellites and one GEO satellite in 2018. At the moment, a single Block I satellite 'Michibiki' is in the commissioning phase, using the L1 C/A, L1C, L2C and L5 signals similar to GPS. The Chinese BDS navigation satellite system is steadily proceeding with the three-step development plan, namely, the buildup of the commissioning system (BDS-1), the regional system (BDS-2) and the global system (BDS-3). So far, three MEO and two IGSO BDS-3 experimental satellites have been launched to support the future full-scale BDS global navigation and positioning service. It is worthwhile to note that the new BDS-3 signals are comparable to GPS Block IIF and Galileo signals in terms of the noise of phase and code observations, which will facilitate the tightly combined precise positioning of new-generation BDS-3, GPS and Galileo. Table 1 summarizes the deployment status of the multi-GNSS constellations, including satellite block types, transmitted signal types and available satellite number, as of September 2017.

2.2 Global ground tracking networks for multi-GNSS real-time processing

From the initialization of the Multi-GNSS Experiment, MGEX observation files are available from the three various repositories hosted by the Crustal Dynamics Data Information System (CDDIS), IGN and BKG archives. As a minimum, all the multi-GNSS stations are required to provide daily observation files with a sampling of 30 s. On top of that, hourly files are delivered by certain stations, roughly three quarters of which support the tracking for a total set of the GPS, GLONASS and Galileo constellations. More than 60 MGEX stations are tracking the BDS satellites at the moment. Thanks to the adequate number of the hourly observation files, the multi-GNSS real-time POD performance can be significantly improved. In order to guarantee the hourly update of ultra-rapid orbit products, an optimized globally distributed multi-GNSS network of about 100 stations that deliver hourly observation files with a sampling interval of 30 s is presented here for the real-time POD solution, as shown in Fig. 1.

Besides the archived hourly data, about half of all IGS multi-GNSS stations also provide real-time data streams through a dedicated BKG caster. In accordance with the prevailing standard for the dissemination of GNSS data, a format called network transport RTCM via internet protocol (Ntrip) is used for streaming the GNSS data to MGEX users. Based on the real-time data streams from the global MGEX and IGS networks and the above-mentioned hourly ultra-rapid orbit products, the PCE solution can be carried out for real-time precise positioning services. Figure 2 shows the global distribution of real-time multi-GNSS tracking stations from the MGEX and IGS networks.

Table 1 Deployment status of the multi-GNSS constellations as of September 2017

System	Blocks	Signals	Sats
GPS	IIR-M	L1C/A, L1/L2 P(Y), L2C, L1/L2 M	7
	IIR	L1C/A, L1/L2 P(Y)	12
	IIF	L1C/A, L1/L2 P(Y), L2C, L1/L2 M, L5	12
GLONASS	M	L1/L2 C/A+P	23
	M+	L1/L2 C/A + P, L3	1
	K	L1/L2 C/A + P, L3	1 + 1[a]
BDS-2	GEO	B1I, B2I, B3I	5 + 1[a]
	IGSO	B1I, B2I, B3I	6
	MEO	B1I, B2I, B3I	3
BDS-3	IGSO	B1I, B3I, B1C, B2a/b	2
	MEO	B1I, B3I, B1C, B2a/b	2 + 1[a]
Galileo	IOV	E1, E6, E5a/b/ab	3 + 1[a]
	FOC	E1, E6, E5a/b/ab	12 + 2[a]
QZSS	I	L1 C/A, L1C, L1-SAIF, L2C, L6-LEX, L5	1

[a]Non-operational satellite

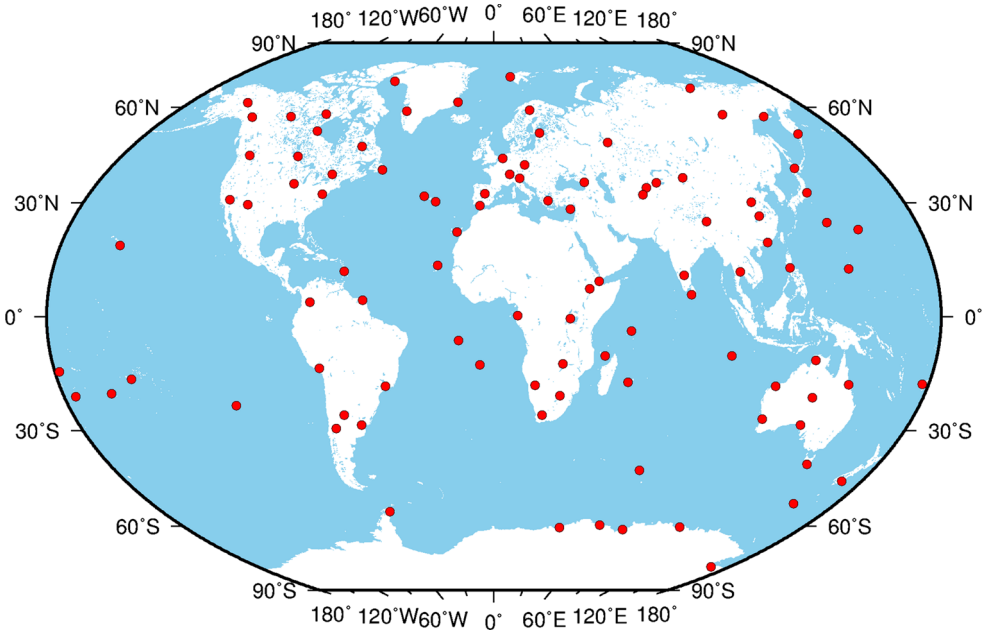

Fig. 1 Global distribution of the tracking stations selected for hourly multi-GNSS POD

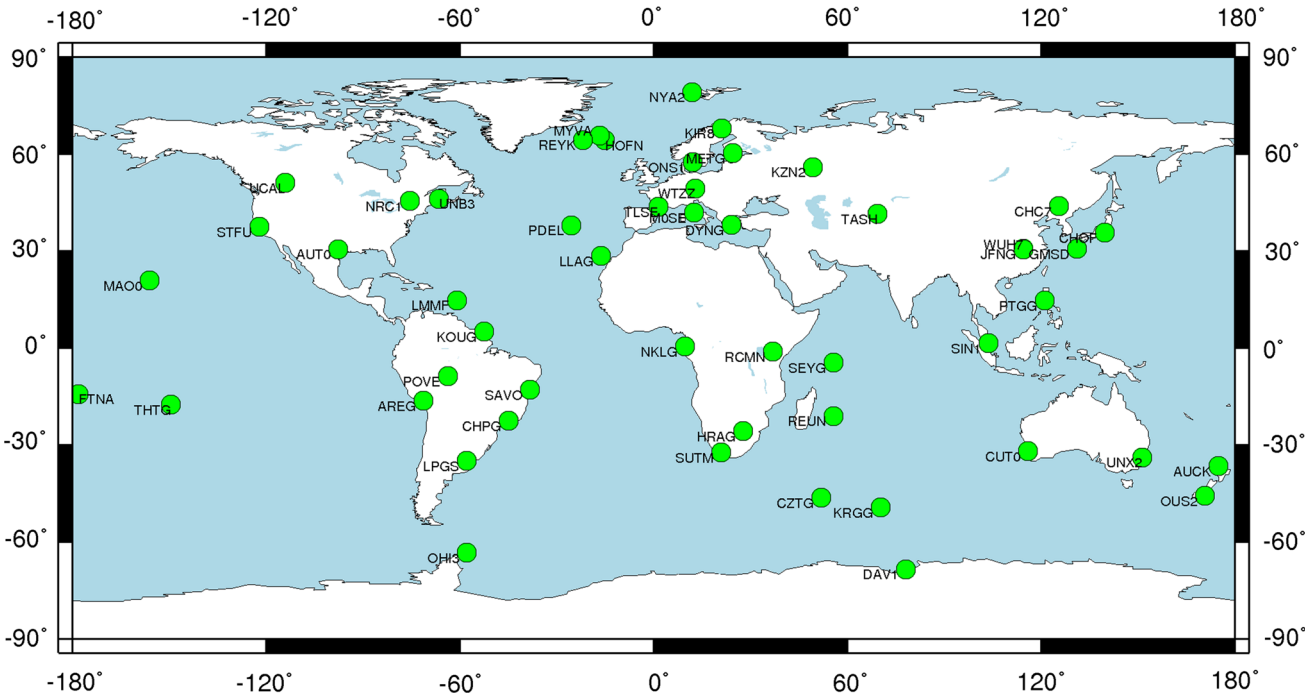

Fig. 2 Global distribution of multi-GNSS stations from MGEX and IGS networks delivering the real-time data stream

3 Multi-GNSS real-time processing

3.1 Multi-GNSS observational model

In general, a multi-GNSS real-time PPP system consists of at least three components including POD, PCE and PPP. In this study, we present a rigorous GPS + GLONASS + BDS + Galileo + QZSS five-system model to fully exploit the observations from all the five navigation satellite systems for real-time POD, PCE and PPP. The raw-observation (Schaffrin and Bock 1988) model for undifferenced (UD) carrier phase L and pseudorange P can be expressed as follows:

$$L_{r,i}^{s} = \rho_{r}^{s} - \Delta t^{s} + \Delta t_{r} + \lambda_{i}(b_{r,i} - b_{i}^{s} + N_{r,i}^{s}) - I_{r,i}^{s} + T_{r}^{s} + \varepsilon_{r,i}^{s} \quad (1)$$

$$P_{r,i}^{s} = \rho_{r}^{s} - \Delta t^{s} + \Delta t_{r} + c \cdot (d_{r,i}^{-} d_{i}^{s}) + I_{r,i}^{s} + T_{r}^{s} + \omega_{r,i}^{s} \quad (2)$$

where indices s, r, and i represent the satellite, receiver, and carrier frequency, respectively; ρ_r^s denotes the geometric distance between the satellite- and receiver-end antenna phase centers at the signal transmitting and receiving time, respectively; Δt^s and Δt_r are the satellite clock bias and the receiver clock bias (unit: m), respectively; λ_i is the wavelength; $b_{r,i}$ and b_i^s are the receiver- and satellite-dependent uncalibrated phase delays (UPDs) (Ge et al. 2008; Li et al. 2017); $N_{r,i}^s$ is the integer ambiguity; c is the speed of light in vacuo; $d_{r,i}$ and d_i^s are the receiver- and the satellite-end code biases at frequency i, respectively; $I_{r,i}^s$ is the frequency-dependent slant ionospheric delay of the signal path; T_r^s is the frequency-independent slant tropospheric delay; $\omega_{r,i}^s$ and $\varepsilon_{r,i}^s$ represent the sum of measurement noise and multipath effects for the pseudorange and carrier phase observations, respectively. In addition, the error components such as phase center offsets and variations, ocean tide loading, earth tide, phase wind-up, differential code biases and relativistic delays must also be corrected with the existing models (Zumberge et al. 1997; Schaer et al. 1999; Liu and Ge 2003; Dach et al. 2006; Steigenberger et al. 2011; Kouba 2009), which are not specified in the observation equations.

Considering the frequency-dependent nature of the ionospheric delay, we can eliminate the first order of ionospheric delays by using the dual-frequency ionosphere-free (IF) combined observations. We will hereafter focus on the IF combined observation equations as follows:

$$l_{r,\mathrm{IF}}^{s} = \boldsymbol{\psi}_{r}^{s} \cdot (\Phi(t,t_0)^{s} \cdot \mathbf{o}_{0}^{s} - \mathbf{r}_{r}) - \Delta t_{\mathrm{IF}}^{s} + \Delta t_{r,\mathrm{IF}} + \lambda_{\mathrm{IF}}(b_{r,\mathrm{IF}} - b_{\mathrm{IF}}^{s} + N_{r,\mathrm{IF}}^{s}) + m_{r,\mathrm{trop}}^{s} \cdot \delta_{r,\mathrm{trop}}^{+} \varepsilon_{r,\mathrm{IF}}^{s} \quad (3)$$

$$p_{r,\mathrm{IF}}^{s} = \boldsymbol{\psi}_{r}^{s} \cdot (\Phi(t,t_0)^{s} \cdot \mathbf{o}_{0}^{s} - \mathbf{r}_{r}) - \Delta t_{\mathrm{IF}}^{s} + \Delta t_{r,\mathrm{IF}} + c \cdot (d_{r,\mathrm{IF}}^{-} d_{\mathrm{IF}}^{s}) + m_{r,\mathrm{trop}}^{s} \cdot \delta_{r,\mathrm{trop}} + \omega_{r,\mathrm{IF}}^{s} \quad (4)$$

$$\mathbf{o}_{0}^{s} = (x_0^s y_0^s z_0^s v_{x_0}^s v_{y_0}^s \; v_{z_0}^s p_1^s p_2^s \ldots p_5^s)^T \quad (5)$$

where $l_{r,\mathrm{IF}}^s$ and $p_{r,\mathrm{IF}}^s$ denote "observed minus computed" IF phase and pseudorange observables from satellite s to receiver r, respectively; $\boldsymbol{\psi}_r^s$ is the unit vector of the direction from receiver to satellite; $\mathbf{r}_r$ is the vector of the receiver position increments relative to an a priori position; $\Phi(t,t_0)^s$ is the state transition matrix from initial epoch t_0 to current epoch t; $m_{r,\mathrm{trop}}^s$ is the related mapping function with respect to the zenith tropospheric wet delays $\delta_{r,\mathrm{trop}}$; $\mathbf{o}_0^s$ denotes the initial orbit state vector of satellite s, including the initial position (x_0^s, y_0^s, z_0^s), the initial velocity ($v_{x_0}^s$, $v_{y_0}^s$, $v_{z_0}^s$) and the five Bern solar radiation pressure parameters (ECOM) (p_1^s, p_2^s, … p_5^s) (Beutler et al. 1994).

The combined GPS + GLONASS + BDS + Galileo + QZSS observation model for POD can be expressed as follows:

$$\begin{cases} l_{r,\mathrm{IF}}^{S} = \boldsymbol{\psi}_{r}^{S} \cdot (\Phi(t,t_0)^{S} \cdot \mathbf{o}_{0}^{S} - \mathbf{r}_{r}) - \Delta t_{\mathrm{IF}}^{S} + \Delta t_{r,\mathrm{IF}} + \lambda_{r_s,\mathrm{IF}}(b_{r_s,\mathrm{IF}} - b_{\mathrm{IF}}^{S} + N_{r,\mathrm{IF}}^{S}) + m_{r,\mathrm{trop}}^{S} \cdot \delta_{r,\mathrm{trop}} + \varepsilon_{r,\mathrm{IF}}^{S} \\ p_{r,\mathrm{IF}}^{S} = \boldsymbol{\psi}_{r}^{S} \cdot (\Phi(t,t_0)^{S} \cdot \mathbf{o}_{0}^{S} - \mathbf{r}_{r}) - \Delta t_{\mathrm{IF}}^{S} + \Delta t_{r,\mathrm{IF}} + c \cdot (d_{r_S,\mathrm{IF}} - d_{\mathrm{IF}}^{S}) + m_{r,\mathrm{trop}}^{S} \cdot \delta_{r,\mathrm{trop}} + \omega_{r,\mathrm{IF}}^{S} \\ S = (G, R_k, E, C, J) \end{cases} \quad (6)$$

where indices G, R, E, J and C refer to the GPS, GLONASS, Galileo, QZSS and BDS satellite system, respectively; R_k denotes the GLONASS satellite with frequency factor k in the frequency division multiple access (FDMA) mode. It should be noted that the international terrestrial reference frame (ITRF 2014) and the GPS time are applied here for all the satellite constellations and station coordinates. In the POD processing, we give strong constraints on the station position estimates by using the IGS published station coordinates of weekly solution in the ITRF 2014.

In the multi-GNSS POD procedure, the IF GPS code biases $d_{r_G,\mathrm{IF}}$ and d_{IF}^s will be absorbed by clock terms $\Delta t_{r,\mathrm{IF}}$ and Δt_{IF}^s, respectively. It is well known that the inclusion of code biases with the clock offsets and using the same clock offsets in the phase equations will introduce the code biases into the phase observation equations. These biases can be absorbed with the float ambiguities (El-Mowafy et al. 2016). The phase delays $b_{r_s,\mathrm{IF}}$ and b_{IF}^s will be coupled with the IF combined integer phase ambiguities term $N_{r,\mathrm{IF}}^s$. Thus, the estimated parameters in the multi-GNSS mode are expressed as follows, including the initial orbit state $\mathbf{o}_0^s$, the station position increments r_r, the satellite clock bias $\Delta\bar{t}_{\mathrm{IF}}^s$, the receiver clock bias $\Delta\bar{t}_{r,\mathrm{IF}}$, the zenith tropospheric wet delay $\delta_{r,\mathrm{trop}}$, the phase ambiguities $\bar{N}_{r,\mathrm{IF}}^s$, the earth rotation parameters δ_{erp} and the inter-system/frequency-dependent code biases relative to the GPS biases $d_{r_G,\mathrm{IF}}$, i.e., $d_{r_{R_k},\mathrm{IF}}$, $d_{r_C,\mathrm{IF}}$, $d_{r_E,\mathrm{IF}}$ and $d_{r_J,\mathrm{IF}}$, at the receiver end.

$$X_{\mathrm{pod}} = \Big(\mathbf{o}_0^{s_1} \ldots \mathbf{o}_0^{s_m},\; \mathbf{r}_r,\; \Delta\bar{t}_{\mathrm{IF}}^{s_1} \ldots \Delta\bar{t}_{\mathrm{IF}}^{s_m},\; \Delta\bar{t}_{r,\mathrm{IF}},\; \delta_{r,\mathrm{trop}}\; \delta_{erp}, \times d_{r_E,\mathrm{IF}},\; d_{r_C,\mathrm{IF}},\; d_{r_{R1},\mathrm{IF}} \ldots d_{r_{R_k},\mathrm{IF}},\; d_{r_J,\mathrm{IF}},\; \bar{N}_{r,\mathrm{IF}}^{s_1} \ldots \bar{N}_{r,\mathrm{IF}}^{s_m} \Big)^T \quad (7)$$

$$\begin{aligned} \Delta\bar{t}_{\mathrm{IF}}^{s} &= \Delta t_{\mathrm{IF}}^{s} + c \cdot d_{\mathrm{IF}}^{s} \\ \Delta\bar{t}_{r,\mathrm{IF}} &= \Delta t_{r,\mathrm{IF}} + c \cdot d_{r_G,\mathrm{IF}} \\ \bar{N}_{r,\mathrm{IF}}^{s} &= N_{r,\mathrm{IF}}^{s} + b_{r,\mathrm{IF}} - b_{\mathrm{IF}}^{s} \end{aligned} \quad (8)$$

In view of the dynamic stability of the satellite movement, the real-time orbit is currently predicted based on orbits determined in a batch least square (LSQ) processing mode. In

this study, the multi-step numerical integration of the equations of motion is used for the orbit prediction, in connection with the dynamic force models including solar radiation pressure (ECOM), Geopotential EGM96 model (12 × 12), solid earth tide, pole tide, ocean tide, M-body gravity model (JPL DE405), and so on. However, the estimation of the real-time satellite clock corrections must be updated as frequently as possible due to their short-term fluctuations (Zhang et al. 2011).

In the PCE procedure, based on the satellite orbit, IFB corrections and station coordinates derived from the real-time POD, the number of estimated parameters is further reduced in order to ensure the high-frequency update of real-time clock corrections (e.g., 5 s for IGS Real-time Pilot Project, RTPP). The multi-GNSS IF observation model and the estimated parameters for PCE are expressed, as follows:

$$\begin{cases} \tilde{l}^S_{r,\mathrm{IF}} = -\Delta\bar{t}^S_{\mathrm{IF}} + \Delta\bar{t}_{r,\mathrm{IF}} + \lambda_{r_S,\mathrm{IF}} \cdot \bar{N}^S_{r,\mathrm{IF}} + m^S_{r,\mathrm{trop}} \\ \qquad \cdot\ \delta^+_{r,\mathrm{trop}} \varepsilon^S_{r,\mathrm{IF}} \\ \tilde{p}^S_{r,\mathrm{IF}} = -\Delta\bar{t}^S_{\mathrm{IF}} + \Delta\bar{t}_{r,\mathrm{IF}} + c \cdot (d_{r_S,\mathrm{IF}} - d_{r_G,\mathrm{IF}}) \\ \qquad + m^S_{r,\mathrm{trop}} \cdot \delta^+_{r,\mathrm{trop}} \omega^S_{r,\mathrm{IF}} \\ S = (G, R_k, E, C, J) \end{cases} \tag{9}$$

$$X_{pce} = \left(\Delta\bar{t}^s_{\mathrm{IF}}\ \Delta\bar{t}_{r,\mathrm{IF}}\ \delta_{r,\mathrm{trop}}\ d_{r_E,\mathrm{IF}}\ d_{r_C,\mathrm{IF}}\ d_{r_{R_k},\mathrm{IF}}\ d_{r_J,\mathrm{IF}}\ \bar{N}^s_{r,\mathrm{IF}} \right)^T \tag{10}$$

where $\tilde{l}$ and $\tilde{p}$, respectively, denote "observed minus computed" phase and pseudorange observations obtained based on the known satellite and station coordinates derived from POD.

With the real-time orbit, clock and DCB corrections at the satellite end, multi-GNSS float PPP can be carried out. The estimated parameters include station coordinates, receiver clock biases, ISB and float ambiguities. Based on the float ambiguities derived from PPP solutions, the satellite-dependent UPDs are estimated and transmitted in real-time mode and thus the real-time UPD products can be used for real-time PPP AR (Li et al. 2013). The IF combined observation model and estimated parameters for multi-GNSS real-time PPP AR can be expressed as,

$$\begin{cases} \bar{l}^S_{r,\mathrm{IF}} = -\boldsymbol{\psi}^S_r \cdot \bar{\mathbf{r}}_r + \Delta\bar{t}_{r,\mathrm{IF}} + \lambda_{r_S,\mathrm{IF}} \cdot N^S_{r,\mathrm{IF}} + m^S_{r,\mathrm{trop}} \\ \qquad \cdot\ \delta_{r,\mathrm{trop}} + \varepsilon^S_{r,\mathrm{IF}} \\ \bar{p}^S_{r,\mathrm{IF}} = -\boldsymbol{\psi}^S_r \cdot \bar{\mathbf{r}}_r + \Delta\bar{t}_{r,\mathrm{IF}} + c \cdot d_{r_S,\mathrm{IF}} + m^S_{r,\mathrm{trop}} \\ \qquad \cdot\ \delta_{r,\mathrm{trop}} + \omega^S_{r,\mathrm{IF}} \\ S = (G, R_k, E, C, J) \end{cases} \tag{11}$$

$$X_{ppp} = \left(\bar{\mathbf{r}}_r\ \Delta\bar{t}_{r,\mathrm{IF}}\ \delta_{r,\mathrm{trop}}\ d_{r_E,\mathrm{IF}}\ d_{r_C,\mathrm{IF}}\ d_{r_{R_k},\mathrm{IF}}\ d_{r_J,\mathrm{IF}}\ N^s_{r,\mathrm{IF}} \right)^T \tag{12}$$

where $\bar{l}$ and $\bar{p}$ denote "observed minus computed" phase and pseudorange observations obtained by using the real-time precise orbit, clock and UPD products, Ψ represents the transition matrix with respect to the position estimates $\bar{\mathbf{r}}_r$ at the user end.

In this study, an elevation-dependent weighting strategy is applied for the combined data processing of multi-GNSS observations. The stochastic model of IF pseudorange and carrier phase observations can be described by Eq. (13):

$$Cov(i, j) = \begin{cases} \sigma^2 & (i = j) \\ 0 & (i \neq j) \end{cases}$$
$$\sigma^2 = a^2 + b^2 \cos^2 E \tag{13}$$

where σ is the standard deviation of the measurements (unit: m); E is the satellite elevation angle (unit: rad); a and b are empirical constants. In the GNSS processing, both a and b are generally set to be 0.009 m for carrier phase and 0.9 m for code observations.

3.2 Multi-GNSS hourly ultra-rapid orbit determination

Providing more precise and reliable ultra-rapid orbit products is critical for multi-GNSS real-time positioning, especially for the three merging constellations BDS, Galileo and QZSS which are still under construction. Recently, most of IGS analysis centers (ACs) select the 1-day POD solution in order to update the ultra-rapid orbit products every 3 h for real-time positioning services and few orbit products contain BDS, Galileo and QZSS. In general, the POD processing should be as fast as possible and the update interval should be as short as possible to reduce the orbit prediction length and guarantee the accuracy of the predicted orbit. However, limited to huge computational burden, the conventional strategy cannot meet the requirement of the hourly update of multi-GNSS POD. In this study, a hourly POD strategy is proposed to improve the orbit accuracy and computation efficiency of POD compared to the conventional case. Even for the 48 h processing, the five-system POD can be completed within 1 h and the hourly multi-GNSS orbit update is achievable. The detailed description of the new strategy is presented in the following.

First of all, the reliable support of multi-GNSS observation and broadcast files is critical for a good performance of ultra-rapid POD. It should be mentioned that all the POD calculations are based on a single Linux server in this study. Considering the computational efficiency of the single-server hourly POD, we selected the globally distributed multi-GNSS network of about 100 stations for the multi-GNSS real-time precise orbit determination, as shown in Fig. 1. The IGS and MGEX data available from the CDDIS, IGN

Table 2 Comparison of old and new strategies used for Multi-GNSS ultra-rapid POD

Item	Old strategy	New strategy
Orbit Update	Every 3 h	Every 1 h
Orbit arc	1-day solution	2-day solution
Processing interval	300 s	600 s
ISB and IFB	ISB and IFB estimated as constant	ISB estimated and IFB corrected
Download and merge observations	Single-thread	Multi-thread
Data preprocessing	Single-thread	Multi-thread
Orbit prediction	Single-thread	Multi-thread
Read and write	Conventional hard drive	Solid state drive

and BKG archives are provided together for multi-GNSS ultra-rapid POD, which certainly guarantees the sufficient number of available observation files. Meanwhile, the real-time broadcast files provided by Technische Universität München (TUM) are further processed for the consistency of the initial orbit (ftp://ftp.lrz.de/transfer/steigenb/brdm/).

To obtain the consistency for different systems, the GPS + GLONASS + BDS + Galileo + QZSS observations from CDDIS + IGN + BKG networks should be processed together in one common procedure, which also imposes a heavy burden on the computational efficiency. Because of the computational burden, the ultra-rapid orbit products are usually updated every 3 h in the standard POD strategy. The real-time orbit accuracy will be compromised by such a long arc length of prediction. Thus, it is necessary to provide a faster update rate of ultra-rapid orbits and thus shorten the prediction length. In order to ensure the hourly update of multi-GNSS POD, the data processing strategy of POD is required to be improved for promoting the computational efficiency and orbit accuracy.

The difference between the two processing strategies is summarized in Table 2, and the flowchart of the new processing strategies for multi-GNSS hourly POD is shown in Fig. 3. Different from the single-thread method involved for the standard strategy, the multi-thread technique is used for downloading, merging hourly FTP files, data preprocessing and orbit prediction, which significantly reduces the preparation and prediction time for POD by close to 60%. As for the least square adjustment procedure, the 2-day solution with a processing interval of 600 s is selected for multi-GNSS POD. In consideration of computational efficiency, IFB products derived over the previous day in post-processing are introduced as known values to reduce the number of estimated parameters in the new solution. The corresponding results will be presented in Sect. 4.1. Taking into account the impressive performance of solid state drive (SSD), the integrated circuit assemblies are used as memory by this solid-state storage device for increasing the reading and writing speed during the adjustment procedure. Compared to the conventional strategy, the time of the least square estimation for ultra-rapid POD can be reduced by a factor of 3.2 due to the new strategy and thus the hourly update of multi-GNSS POD is achievable, as shown in Fig. 4.

4 Results

In this section, we verify the feasibility of the proposed POD strategy and assess the precision of our multi-GNSS hourly ultra-rapid orbit. Subsequently, the contribution of multi-GNSS to real-time PPP AR and the corresponding positioning performance of multi-GNSS real-time PPP AR are evaluated in Sect. 4.2. In our processing, the PANDA (Ge et al. 2012; Liu and Ge 2003) and iPPP (Li et al. 2013) softwares are used.

4.1 Assessment of multi-GNSS hourly orbit product

Due to the dynamic stability of the satellite movement, the ultra-rapid orbit is predicted based on the orbit estimation part determined by using the latest available observations. With increasing orbit arc length, more GNSS observations are introduced into the orbit estimator to ensure the estimated orbit accuracy, which can positively influence the predicted orbit part especially for the new satellite constellations. However, this will result in a heavy computational burden for multi-GNSS POD, reduce the update rate of ultra-rapid orbit products and thus degrade the predicted orbit accuracy. To promote the computational efficiency and guarantee the orbit accuracy, an appropriate arc length should be determined for multi-GNSS POD. Therefore, we evaluated the impact of different arc lengths on the orbit accuracy of different satellites systems by processing 1 month's data of February in 2017. In this study, the 18-h overlap of estimated parts from two adjacent POD processing is used for the assessment of ultra-rapid orbits. Figure 5 shows the averaged root mean square (RMS) values of 18-h overlapping orbit differences in along-track, cross-track and radial component for five navigation

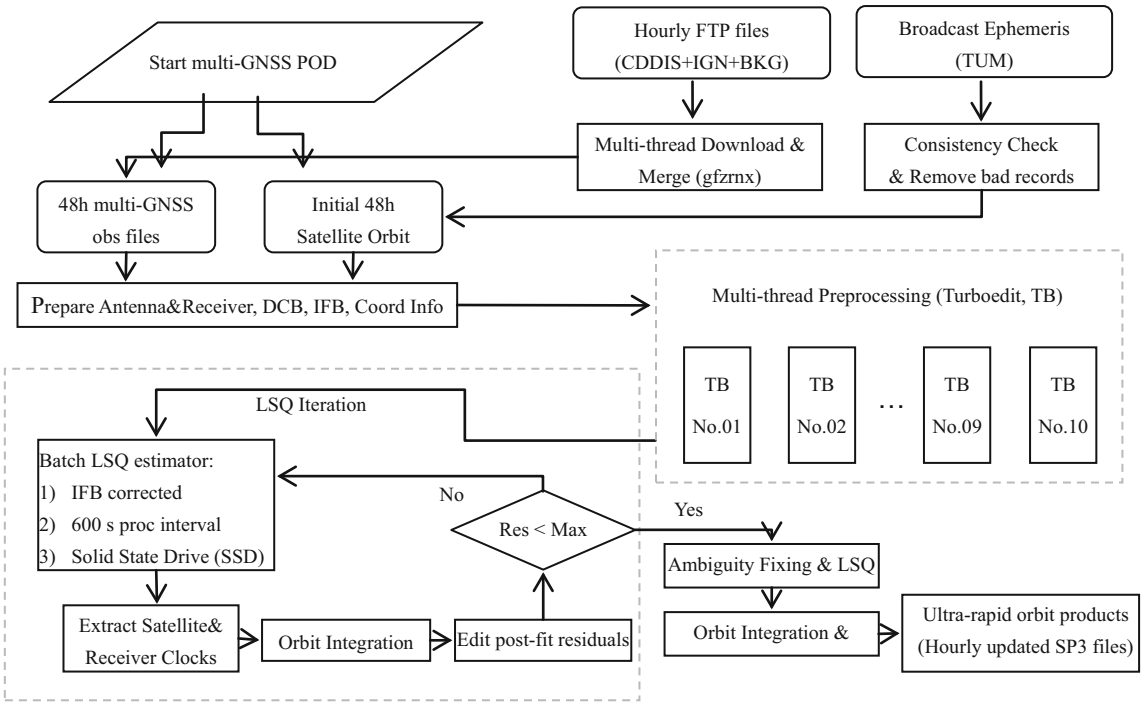

Fig. 3 Improved processing strategy for multi-GNSS ultra-rapid POD

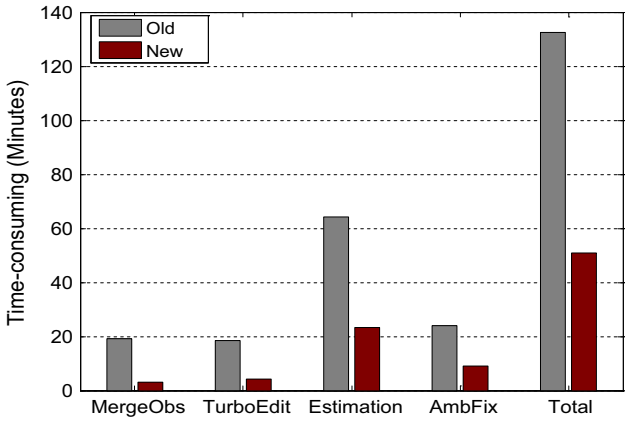

Fig. 4 Comparison of old and new processing strategies for multi-GNSS POD in terms of computational efficiency by using MGEX and IGS observation data during the period from April 23, 2017 to May 23, 2017, based on the Linux servers (CPU max MHz: 4000.00, CPU min MHz: 1200, CPU cores: 6, total memory: 65,861,652 kB) at GFZ

satellite systems with different arc lengths. Because of the dynamic stability of satellite movements, there is no big difference between the 2.5 and 3-day POD solution. For the arc lengths of more than 3 days, the GNSS ultra-rapid orbits are comparable to each other. In addition, the 2-day solution can exactly achieve the hourly update of orbits instead of the 1 or 1.5-day solution, considering the current computational efficiency. Thus, we selected the processing arc lengths of 1, 2 and 3 days for comparison of GNSS orbits. For the orbit arcs of 1, 2 and 3 days, the achieved orbit accuracy of GPS and GLONASS satellites is comparable to each other since GPS and GLONASS are well supported worldwide. With the development of the MGEX global network, the Galileo tracking stations accounts for around 75% of the total selected GNSS network, contributing to the Galileo POD solution. In the case of the arc length of 2 days, the overlap RMS values of Galileo satellites are about 1.2, 2.2 and 4.0 cm in radial, cross-track and along-track components, respectively. Unlike Galileo, BDS is not well observed in several parts of the world, e.g., in the Northern Pacific and Northern Asia region. Apart from the limited availability of BDS tracking stations, the orbit accuracy of BDS satellites will also be negatively affected by a geometric observability limitation for the GEO and IGSO satellites. For the orbit arc of 2 days, the averaged RMS values of BDS IGSO satellites are about 2.9, 3.2, 7.3 cm in radial, cross-track and along-track components, respectively, and the averaged RMS values of BDS MEO satellites are about 2.0, 3.1, 6.2 cm in the three components, respectively. The overlap RMS values of BDS GEO satellites are about 4.5 and 4.7 cm in the radial and cross direction, while the along-track accuracy of GEO satellites is clearly worse than for both, the IGSO and MEO satellites, since the GEO satellites do not move significantly in the along-track component with respect to the ground stations. As QZSS tracking stations only cover the East-Asia and Western Pacific regions, the averaged overlap RMS values are about 2.3, 8.0, 10.2 cm for the 2-day solution in the

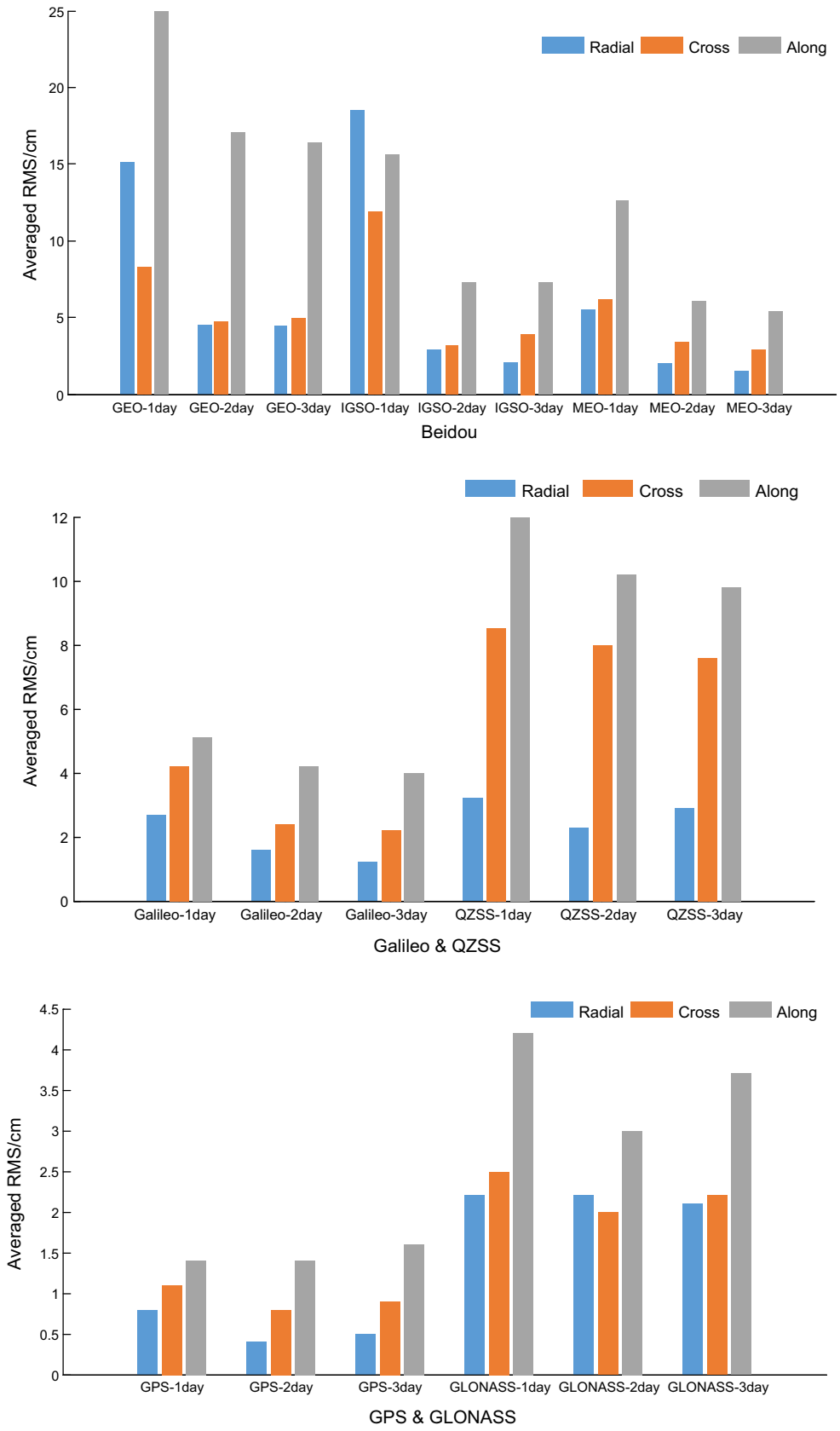

Fig. 5 Averaged RMS values (cm) of 18-h orbit overlap differences in radial, cross, and along directions for multi-GNSS POD with different arc length

radial, cross and along direction, respectively, worse than for the other systems except BDS GEO. For BDS, Galileo and QZSS satellites, the orbit accuracy of the 2-day solution is very close to that of 3 days, which is much better than the 1-day solution. Considering the present POD computational efficiency and orbit accuracy, the arc length of 2 days is chosen for multi-GNSS POD in our study.

For improving the POD computational efficiency and guaranteeing the orbit accuracy, we properly extend the processing interval for multi-GNSS POD. Here, the 2-day POD solution with processing interval of 600 s is carried out compared to that with the 300 s interval. In order to assess the quality of predicted ultra-rapid orbits, the 6-h predicted part of one arc is compared to the 6-h overlapping arc of the adjacent POD processing. Figure 6 shows the averaged overlap RMS values of 6-h predicted orbit differences in radial, cross-track and along-track components for multi-GNSS POD with different sampling intervals (300 vs. 600 s). Generally, the predicted orbit accuracy is several centimeters worse than the estimated orbit. For a sampling interval of 600 s, the predicted orbit accuracy of Galileo, GLONASS and GPS is comparable to that for a 300 s sampling interval, as shown in Fig. 6. As BDS and QZSS are not well supported in several specific regions, there is a slight difference, not exceeding 1 cm, in the predicted orbit accuracy between the 600 and 300 s sampling interval. Since the performance of multi-GNSS POD with 600 s of processing interval is comparable to that with 300 s interval, it is possible to select a 600 processing interval for the 2-day POD solution in order to reduce the POD computational burden and guarantee the predicted orbit accuracy.

The code biases with respect to GPS are different in one multi-GNSS receiver due to the different frequency and signal structure. Unlike the other systems, GLONASS uses FDMA to make the signals distinguishable from the individual satellites. Consequently, the inter-system biases (ISB) and inter-frequency biases (IFB) must be considered in the multi-GNSS POD solution. In the conventional POD strategy, ISB and IFB have to be estimated as constants for each station and the zero mean conditions are introduced over all the ISB and IFB parameters solving for the rank deficiency of normal equations. With the increase in the number of estimated parameters, the prolonged process time cannot satisfy the requirement of hourly orbit update. Fortunately, we can minimize the number of the estimated parameters by fixing the IFB parameters to the values derived for the previous day in post-processing. Figure 7 shows the averaged overlap RMS values (cm) of 6-h predicted orbit differences in radial, cross and along directions for comparison between multi-GNSS POD with IFB corrected from well-known values and that with IFB estimated as constants. The results confirm that the performance of POD with the IFB a priori correction is equivalent to that with IFB estimated. For the 2-day POD solution with 600 s processing interval, the maximum difference between the two cases is still at the mm-level. Thus, it is feasible for the multi-GNSS POD to only consider the estimation of ISB parameters and use the priori values to correct the IFB part.

The IFB a priori corrections are derived in a general daily post-processing batch mode. Based on the IFB products, we achieve the hourly update of ultra-rapid orbits, the predicted part is used for real-time positioning services. To evaluate the real-time orbit accuracy derived from the two strategies listed in Table 2, the GBM (GFZ) MGEX final orbit products are used as references for comparison. Figure 8 shows the averaged RMS values of orbit differences with the GBM in radial, cross and along directions for the BDS, Galileo, QZSS, GLONASS and GPS satellites over a period of a month from April 23, 2017, to May 23, 2017.

For the GPS satellites, in the case of the optimized POD, the RMS values in the radial, cross and along directions are mostly better than 2.5, 4.0 and 9.0 cm, respectively, and the averaged RMS values for all GPS satellites are 2.1, 3.9 and 8.0 cm, respectively. In contrast, the speed of orbit update for the conventional POD is not comparable to that for the new case due to lower computational efficiency. Hence, the corresponding RMS values for all GPS satellites are worse than that in the optimized POD solution, and the orbit accuracy of GPS satellites can be improved by 30.0, 23.5 and 26.6% in the radial, cross and along directions, respectively, due to the optimized POD strategy.

For the GLONASS satellites, the averaged RMS values for the optimized POD are 2.3, 3.9 and 9.1 cm in the radial, cross and along directions, respectively, and the corresponding improvements of orbit accuracy can reach up to 30.3, 25.0 and 37.7%, respectively, compared to the conventional case. For the optimized multi-GNSS POD, the achieved orbit accuracy of GLONASS satellites is slightly worse than that of GPS satellites due to the difficulty in the GLONASS ambiguity resolution (float solution here for GLONASS).

For the Galileo satellites, the averaged RMS values for the optimized strategy are, respectively, 9.1, 13.1 and 13.4 cm in the radial, cross and along directions, which is 29.5, 6.3 and 59.0% better than the conventional case, respectively. The averaged RMS values of BDS IGSO satellites for the optimized POD are 10.3, 16.0 and 29.8 cm in the radial, cross and along directions, respectively, which is slightly worse than the Galileo results. Compared to the conventional case, the orbit accuracy of BDS IGSO in the three directions can be improved by about 82.4, 47.3 and 49.6%, respectively. In the case of the optimized POD, the averaged RMS values of BDS MEO satellites in the radial, cross and along directions are 4.8, 9.5 and 14.1 cm, respectively. Owing to the new POD strategy, the improvement of orbit accuracy in the three directions can reach about 50.5, 19.5 and 53.7%, respectively.

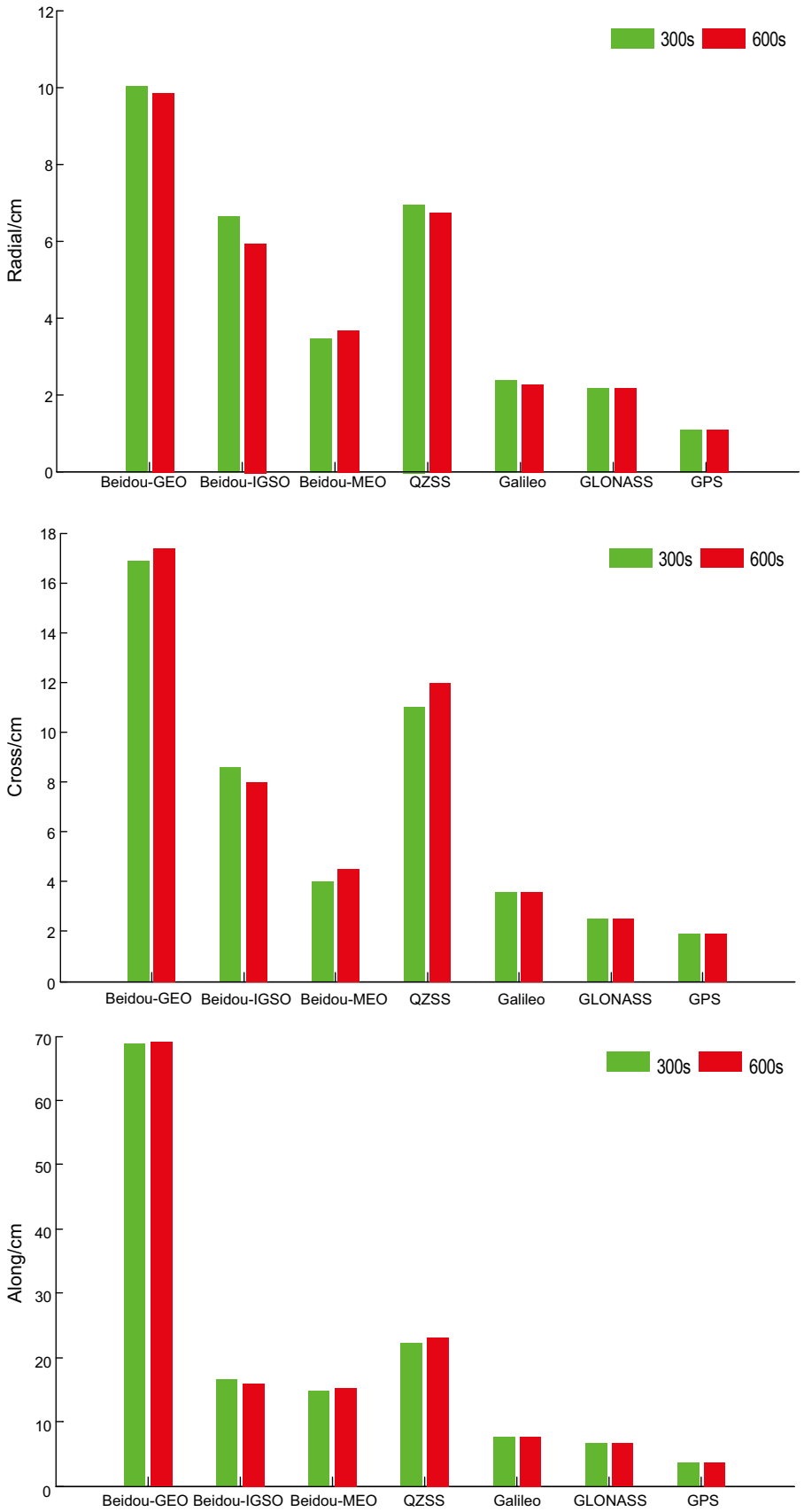

Fig. 6 Averaged overlap RMS values (cm) of 6-h predicted orbit differences in radial, cross, and along directions for multi-GNSS POD with different sampling interval (300 vs. 600 s)

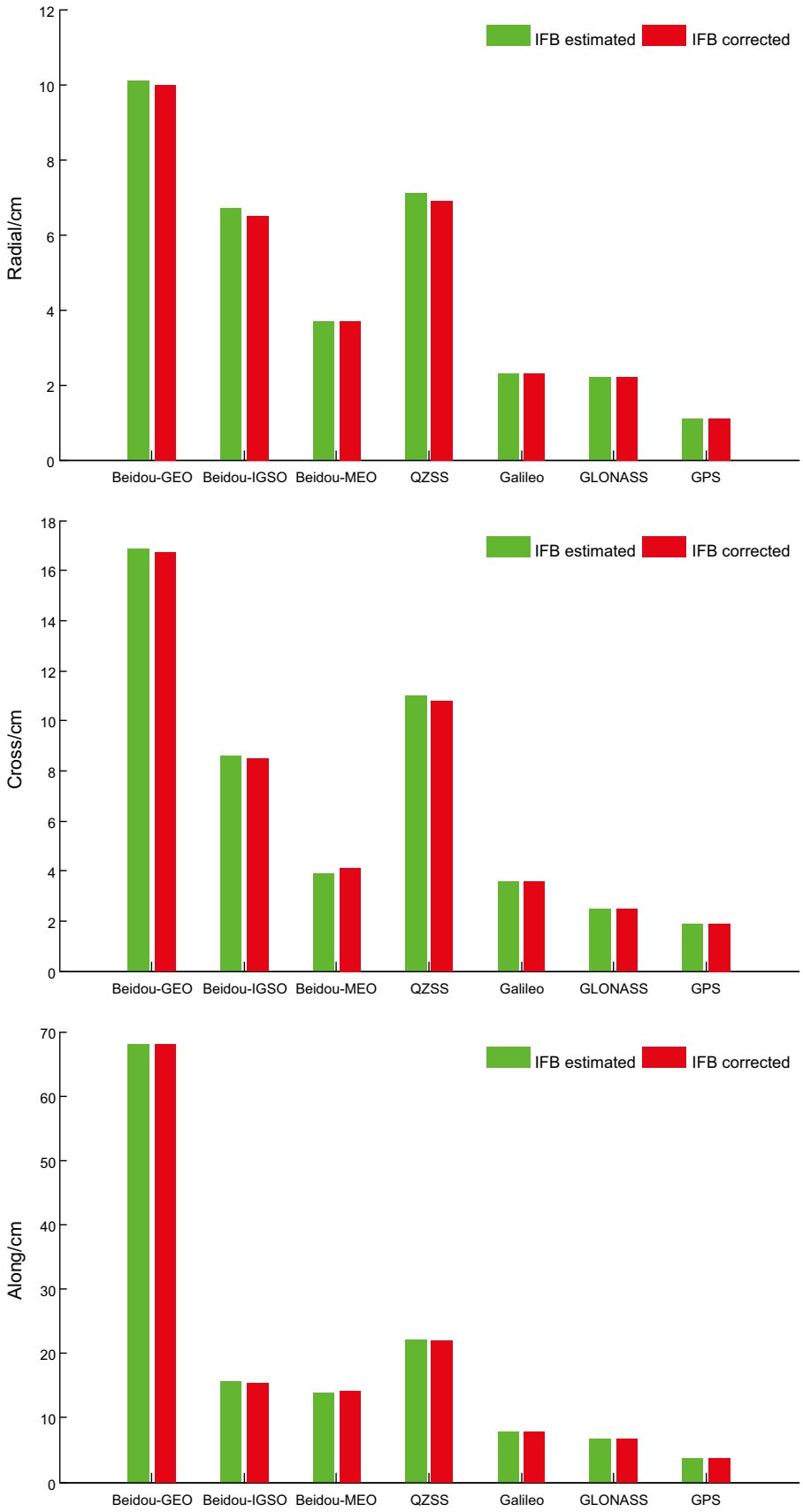

Fig. 7 Averaged overlap RMS values (cm) of 6-h predicted orbit differences in radial, cross, and along directions for multi-GNSS POD with different IFB processing strategies (IFB estimated vs. IFB corrected)

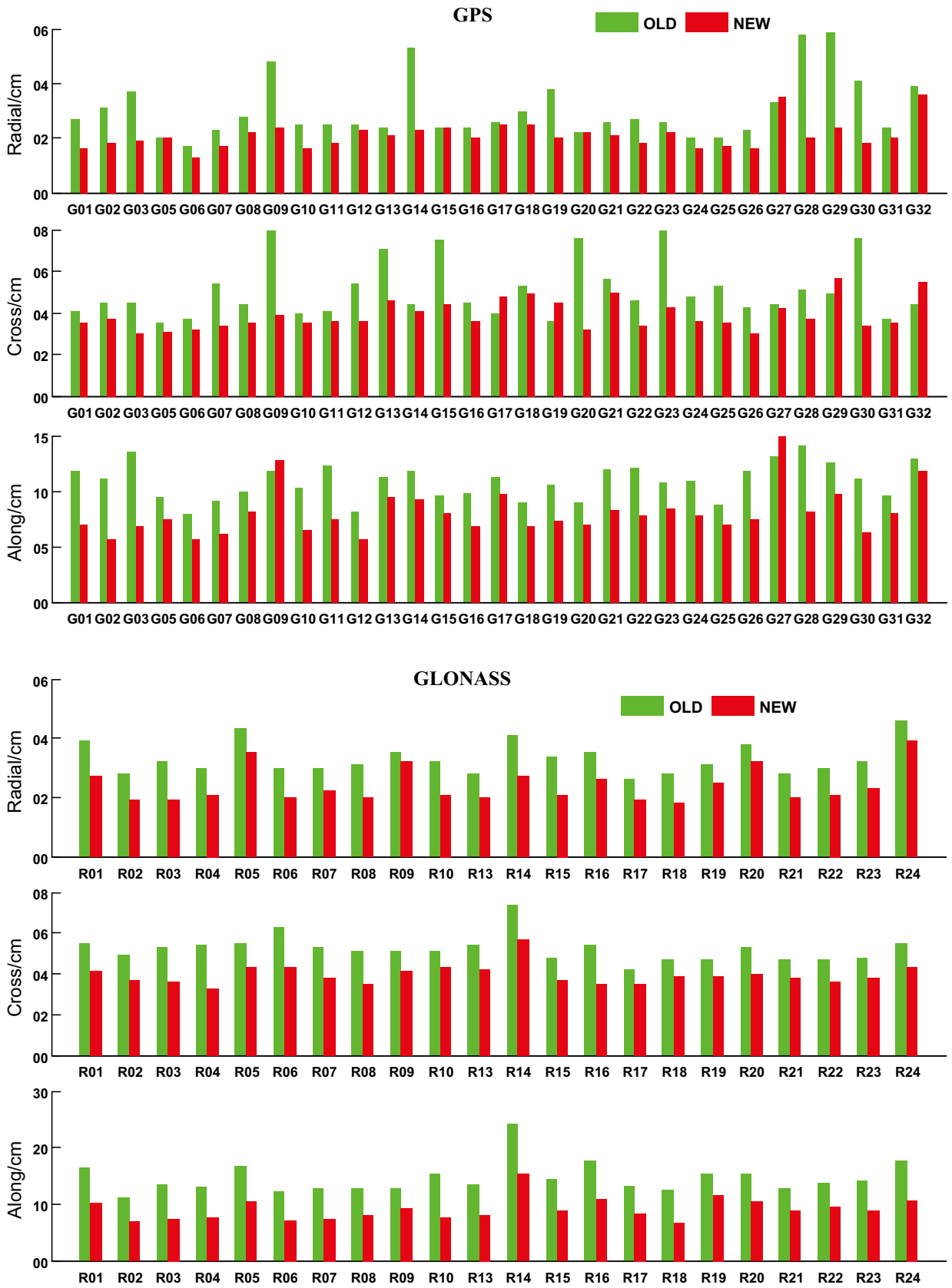

Fig. 8 Averaged RMS values of orbit differences with respect to GMB precise products in radial, cross, and along directions for different multi-GNSS POD strategies over the period from April 22, 2017 to May 23, 2017

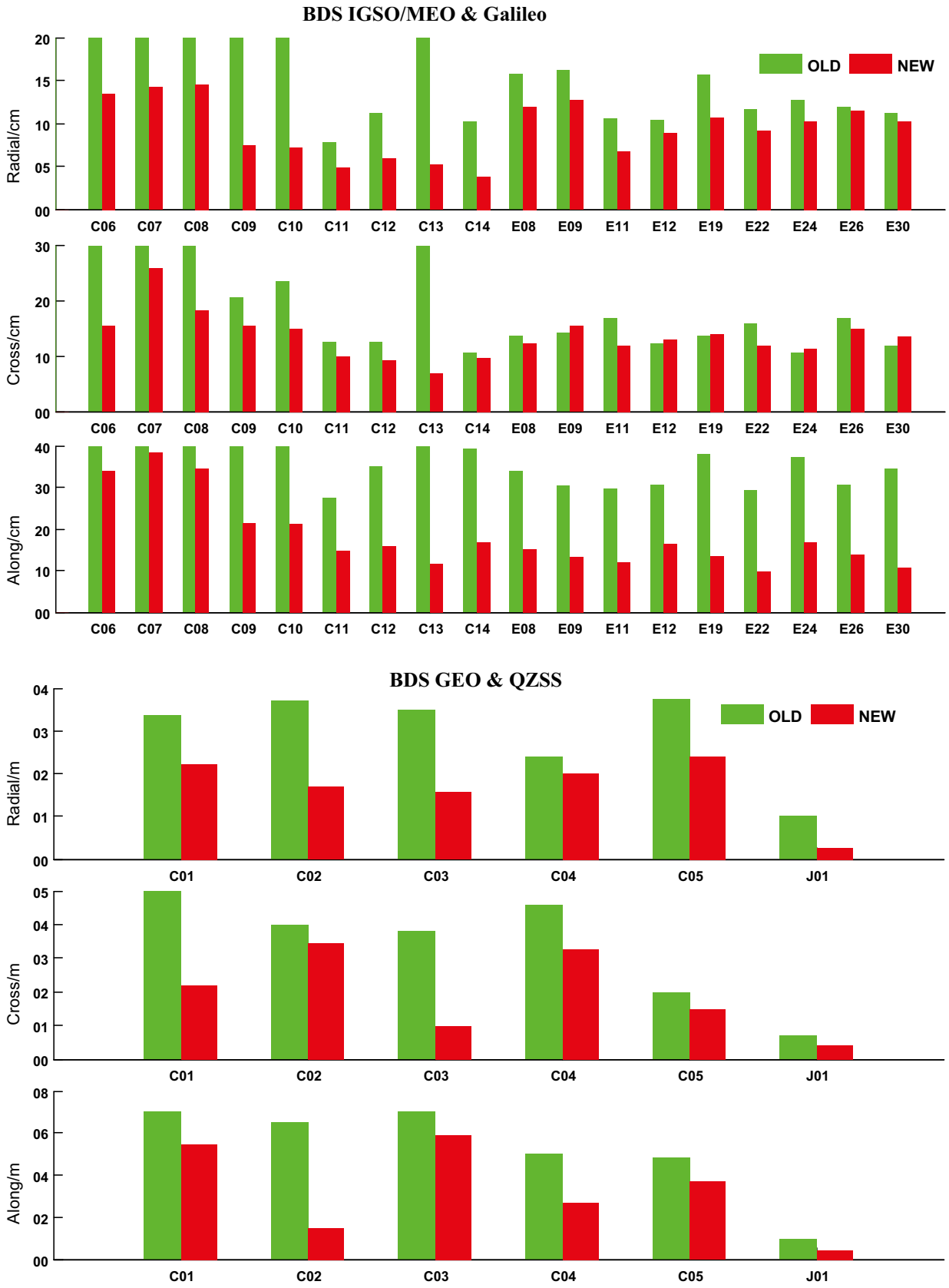

Fig. 8 continued

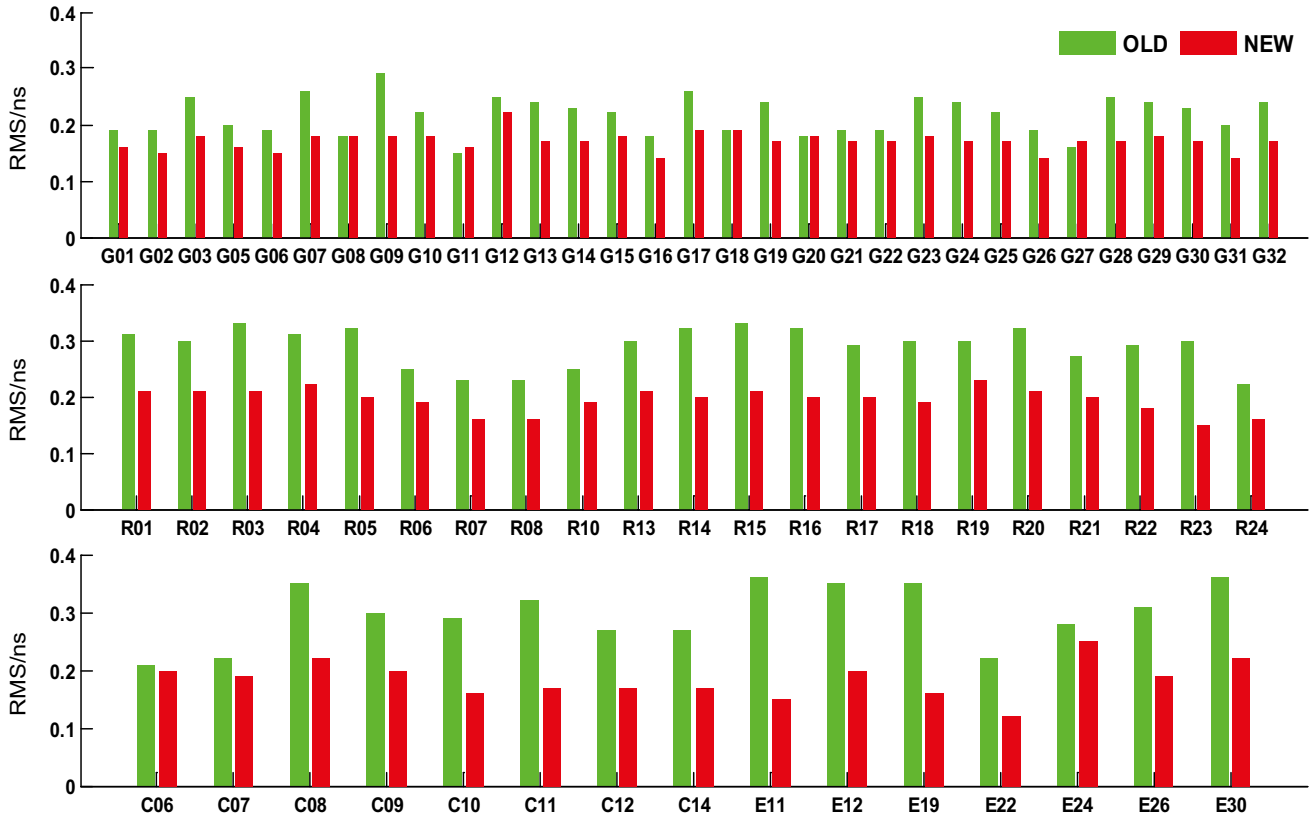

Fig. 9 Averaged RMS values (ns) of clock differences with respect to GMB precise products for different multi-GNSS POD strategies (old POD vs. new POD) over the period from April 22, 2017, to May 23, 2017

Due to the limited observational geometry and the limited distribution of ground tracking stations, the real-time orbit accuracy of BDS GEO and QZSS satellites is much worse than that of other satellites. However, with the optimized POD strategy, the orbit accuracy for BDS GEO satellites in the radial, cross and along directions can be improved by about 56.1, 50.5 and 52.4%, respectively. The averaged RMS values of the QZSS satellite are 27.1, 39.7 and 43.7 cm in the radial, cross and along directions, respectively. The improvement of orbit accuracy for the QZSS satellite in the three directions can reach about 70.5, 43.2 and 55.2%, respectively.

With the real-time orbits hold fixed, the real-time multi-GNSS satellite clock corrections must be estimated and updated frequently due to their short-term fluctuation. To evaluate the accuracy of the real-time clock products for different POD strategies, the post-processed final precise clock products (GBM) provided by GFZ are used for comparison. Figure 9 shows the RMS values of clock differences between the real-time and post-processed products for different POD strategies (old POD vs. new POD strategy as described in Table 2) over the 1 month period from April 22, 2017, to May 23, 2017. The RMS value of the clock difference is taken as clock quality indicator. It should be mentioned that the BDS GEO and QZSS satellite clocks cannot be precisely estimated in real-time mode at present due to the sparse amount of the available tracking data stream. For PCE using the 3-h updated orbit products generated in the conventional POD solution, the average RMS values for the GPS, GLONASS, BDS and Galileo satellites are about 0.22, 0.29, 0.27 and 0.32 ns, respectively. In the case of PCE using the hourly ultra-rapid products from the optimized POD, the RMS values are generally better than 0.2 ns. The averaged RMS value for all the GPS satellites is 0.17 ns. The clock accuracy of about 0.20 ns of the GLONASS, BDS and Galileo satellites is comparable to that of the GPS. The results confirm that by providing hourly ultra-rapid orbits an accuracy of better than 6 cm can be achieved for the GNSS satellite clocks in real-time.

4.2 Multi-GNSS real-time PPP performance

In order to evaluate the impact of improved ultra-rapid orbits on real-time positioning, the high-rate data at the IGS station NNOR with a sample interval of 1 s are processed in a kinematic PPP mode using different real-time orbits derived from the two POD strategies listed in Table 2. The IGS published coordinates of weekly solution are taken as reference

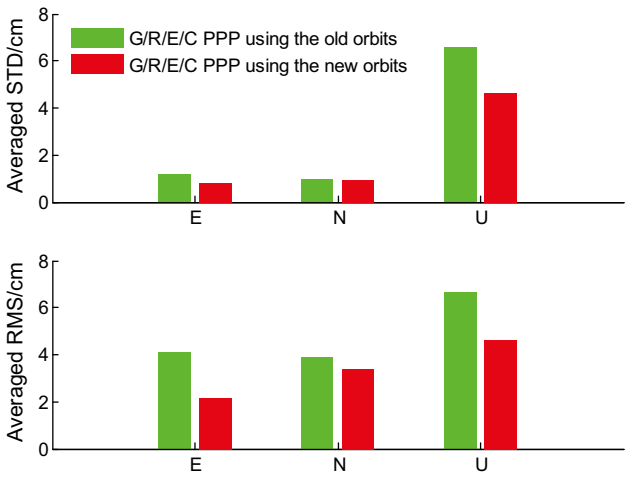

Fig. 10 Averaged STD and RMS values of positioning errors for multi-GNSS float PPP using different real-time orbits (derived from old and new POD, respectively) at station NNOR, over a period from April 19, 2017, to May 23, 2017

for comparison. Figure 10 shows the averaged STD and RMS values of positioning errors relative to the IGS reference coordinates at station NNOR for a four-system combined PPP by using the two predicted orbits over a period from April 19, 2017, to May 23, 2017. The accuracy of multi-GNSS PPP can be improved by 48.2, 13.1 and 30.6% in the east, north and up components, respectively, due to the real-time orbits derived from the new POD. Thus, the following multi-GNSS real-time PPP AR will be investigated based on the optimized predicted orbits and UPD products.

For assessing the contribution of multi-GNSS to PPP AR, 11 stations from MGEX are selected as user stations. The float and fixed PPP in single-, dual- and four-system modes are carried out in parallel. The TTFF, positioning accuracy and fixing percentage are calculated as critical indicators for the assessment of the kinematic PPP AR performance. And we also evaluate and analyze the convergence time and positioning accuracy of float solutions for comparison. In our study, the convergence time is defined as the time to obtain a converged solution with the positioning accuracy of better than 10cm in horizontal components and the fixing percentage is defined as the percentage of fixed sessions over the total number of sessions. All the estimated station coordinates are compared with the SINEX or weekly solution to assess the positioning accuracy. Besides, we also investigate and analyze the performance of kinematic PPP AR under different cutoff elevation angles (from 7° to 30°) and different session lengths (10, 20, 30, 60 and 120 min). In our PPP AR processing, the station coordinates and receiver clock are estimated epoch-by-epoch without any constraints between the epochs. The zenith tropospheric delay (ZTD) is estimated as piecewise constant value every 120 min. The real-time satellite orbits and clocks are derived from the above-mentioned products.

Figure 11 presents the typical results for single-system (GPS), dual-system (GR, GC, GE) and four-system (GCRE) kinematic PPP at the CKIS station on DOY 001, 2017. We can see clearly from Fig. 11 that PPP-AR can significantly shorten the convergence time compared to the float solutions. And the convergence time of dual-system PPP-AR solution is shorter than that of GPS-only solution. Furthermore, GCRE PPP AR solution can achieve shortest convergence time and highest positioning accuracy because of the increment of visible satellites and the improvement in geometry structures.

Figure 12 shows the results of PPP AR solutions for GPS-only, GR and GCRE from 9:00 to 14:00 at station BOR1 selected as the typical case. It becomes obvious that the TTFF of GPS-only PPP AR solution is longer than 30 min for all sessions and the ambiguity resolution of GPS-only even cannot be achieved from 13:00 to 14:00. In contrast, multi-GNSS fixed solution has a shorter TTFF of less than 20 min for all sessions. Especially, the shortest TTFF and highest accuracy can be achieved by GCRE four-system PPP AR results.

We also evaluated the performance of single-, dual- and four-system kinematic PPP AR solutions under different cutoff elevations ranging from 7° to 30°. The results for station DUND are presented in Fig. 13 as a typical example. With the increment of elevation mask, the accuracy of GPS-only PPP AR solutions decreases dramatically. Particularly when cutoff elevation is 30°, GPS-only PPP AR solutions become very unstable and cannot provide continuous precise positioning results, while few centimeters accuracy in horizontal components can still be achieved by GCRE kinematic PPP AR solutions in a short time.

The average convergence periods of the float solution and TTFF of the ambiguity fixed solution for all stations under different cutoff elevation angles are calculated and shown in Fig. 14. In terms of the float solutions, there is a significant decreasing trend in convergence time for all solutions with cutoff elevation angle increasing from 7° to 15°. When the cutoff elevation reaches 30°, the convergence time of the GPS-only, GR, GE and GC PPP increases to 135.3, 58.8, 125.7 and 51.8 min, respectively. Meanwhile, the convergence time of GCRE float solutions is only 20.5 min. With regard to fixed solutions, generally, TTFF of all fixed solutions is much shorter than the convergence time of the corresponding float solutions. And TTFF of single-, dual- and four-system increase with an increasing cutoff elevation angle. The results show that GCRE four-system positions outperform single- and dual-system positions in terms of TTFF and usually presents the shortest TTFF, which is less than 20 min under different cutoff elevation. When the cutoff elevation is increased from 7° to 30°, TTFF of GPS-only, GR, GE and GC results is increased to 118.5, 49.4, 76.3 and 47.1 min, respectively, while TTFF of GCRE fixed solutions

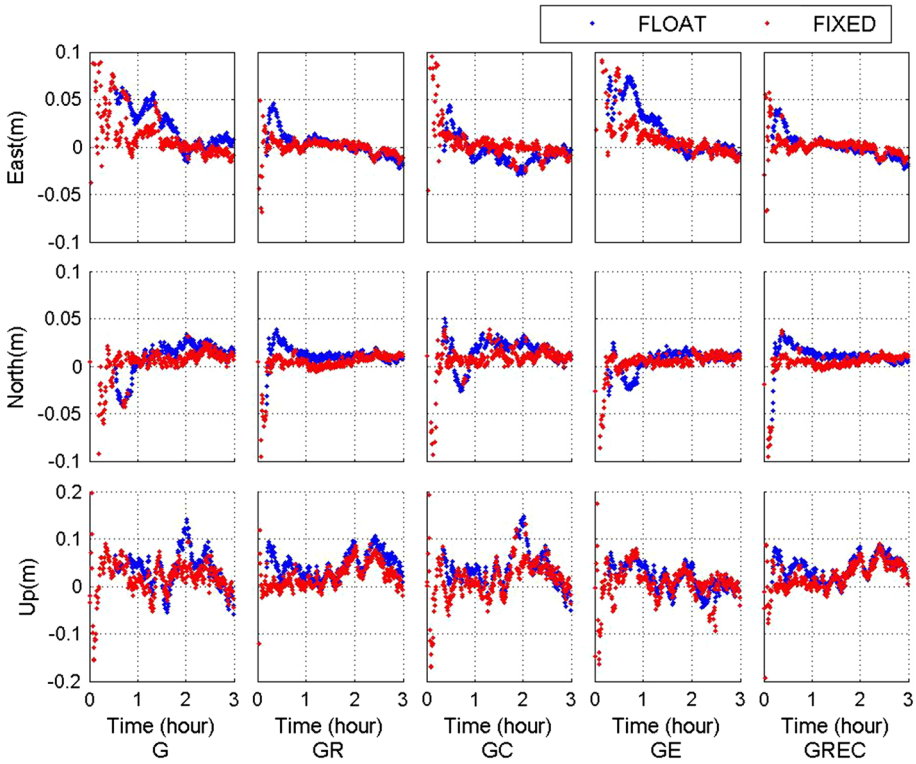

Fig. 11 Float and fixed solutions for GPS, GR, GC, GE and GCRE PPP in kinematic mode at station CKIS, on DOY 001, 2017. Blue and red scatter denote float and fixed solutions, respectively

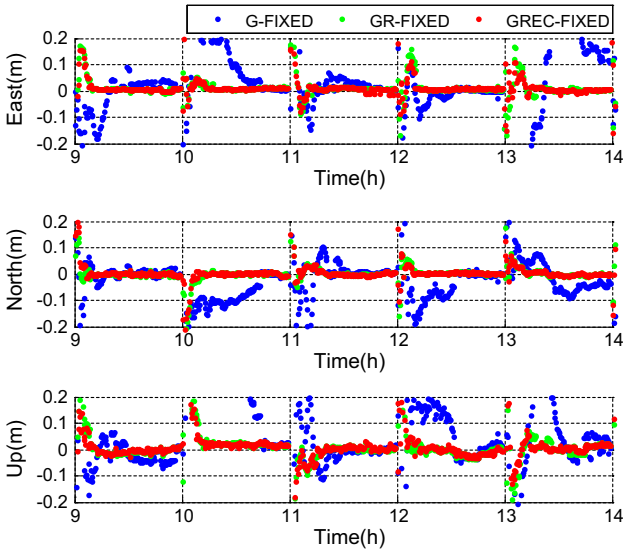

Fig. 12 Kinematic PPP AR results of GPS-only, GR and GCRE at BOR1 station from 9:00 to 14:00 on DOY 1 of 2017

is still stable and shorter than 20 min even at the 30° cutoff elevation.

Figure 15 shows the statistical results of the kinematic PPP solutions with different session lengths, of 10, 20, 30, 60 and 120 min. The RMS values are calculated from all kinematic PPP solutions over all the selected stations and days. The RMS of the float solution is shown in the left sub-figure, and the RMS of fixed solution is shown in the right sub-figure. As we can see from Fig. 15 that along with the increment of observational length, there is an evidently improvement in the positioning accuracy of both float and fixed solutions for the single-, dual- and four-system cases. With the same observational length, the positioning accuracy of PPP AR solutions is higher than that of float solutions. GCRE PPP can achieve the highest positioning accuracy with the same session length, while GPS-only PPP performs worse than the GCRE PPP for both the float and fixed solutions. However, it should be noted that GPS-only PPP might perform better than a GLONASS-only PPP or even a Galileo-only PPP but these cases were not tested here. Moreover, the position accuracy of the north component is better than that in the east and vertical components. Obviously, compared with single-system and dual-system, the GCRE four-system combination significantly improves the performance of PPP AR especially with short session length. GCRE PPP AR solutions can usually achieve the accuracy of few centimeters in three directions only after 20 min, while single- and dual-system PPP requires 30 min and even longer. Within 10 min, the RMS of GCRE PPP AR solutions is 3.66, 2.34 and 7.12 cm, respectively, for the east, north and vertical components while the RMS of GPS-only results is 4.96, 4.08 and 13.77 cm for three components.

The average fixing percentage of kinematic PPP AR solutions over all the selected stations with different session lengths are presented in Fig. 16. It is clearly seen that the fixing percentage of all solutions is improved gradually with

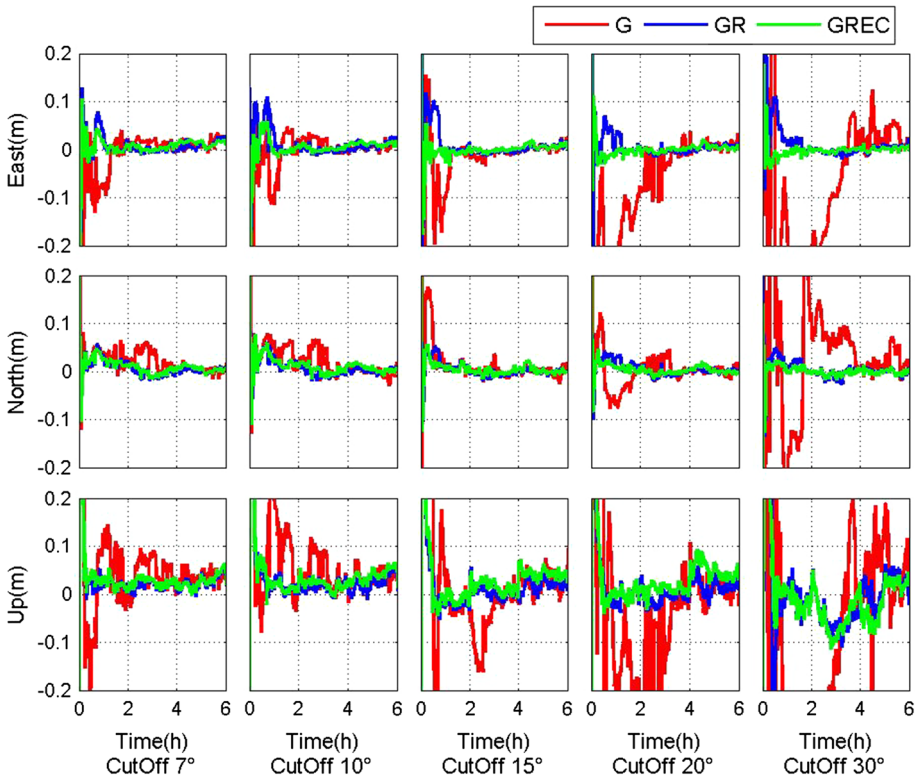

Fig. 13 Kinematic PPP AR results for GPS, GR and GCRE under different cutoff elevation angles at the station DUND on DOY 001, 2017

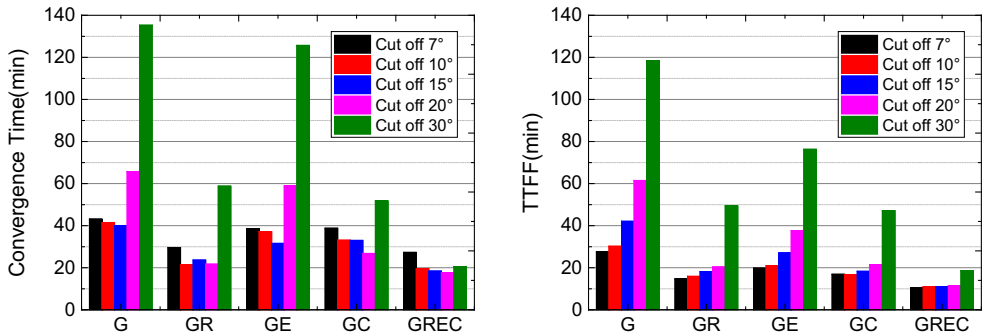

Fig. 14 Averaged convergence time in the kinematic PPP float solutions and the averaged TTFF in the kinematic PPP fixed solutions for G, GR, GE, GC and GCRE under different cutoff elevation angles (7°, 10°, 15°, 20° and 30°)

increasing observation length. With the same observational session length, GCRE four-system PPP AR usually presents the highest fixing percentage while GPS-only PPP AR shows the lowest fixing percentage. Within 10 min, the fixing rate for GPS-only kinematic PPP solutions is only 27.3% while the dual-system fixing rate is 43.3, 46.1 and 60.1%, respectively, for GE, GC and GR. Compared to the single- and dual-system cases, the fixing rate of GCRE PPP AR results increases evidently to about 70.0%. For an observation length of 20min, the fixing percentage of GPS-only, GE, GC, GR and GCRE kinematic PPP AR solutions is, respectively, 52.1, 70.0, 77.7, 87.0, 91.2%. We can see clearly that the GCRE four-system solution provides a significant improvement in terms of the fixing rate, particularly over short session lengths.

5 Conclusions

In this study, we make full use of the GPS + GLONASS + BDS + Galileo + QZSS hourly observations from CDDIS + IGN + BKG archives to implement the hourly multi-GNSS ultra-rapid orbit update. The results show that, with the new POD strategy, the real-time orbit accuracy can be improved for all the satellites compared to the conventional solution. Owing to the new POD strategy, the orbit accuracy of BDS

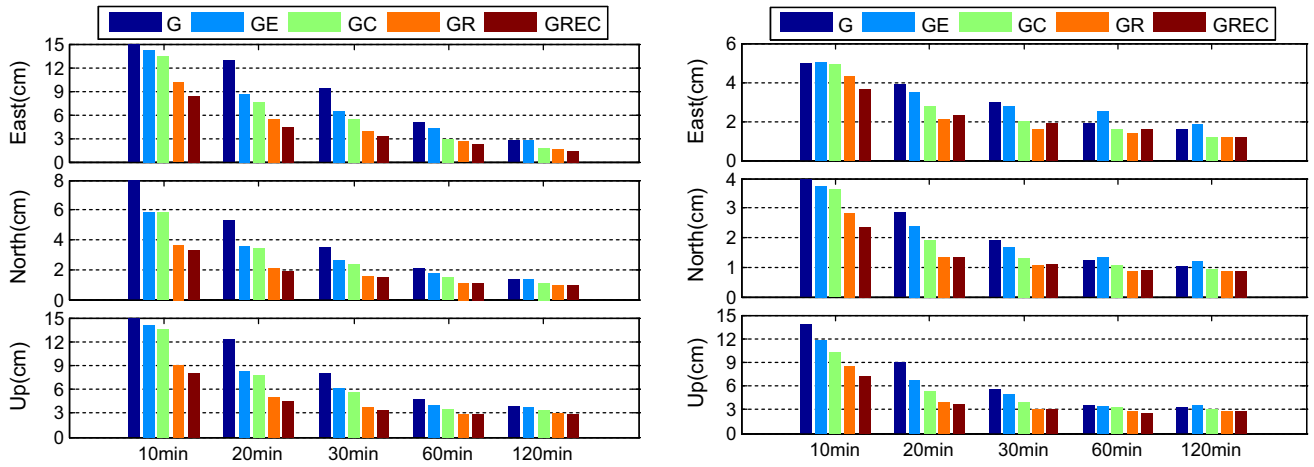

Fig. 15 RMS values of kinematic PPP solutions with different session lengths (10, 20, 30, 60 and 120 min) in single-, dual- and four-system modes. The left sub-figure shows the RMS of the float solutions, and the right shows the RMS of the fixed solutions

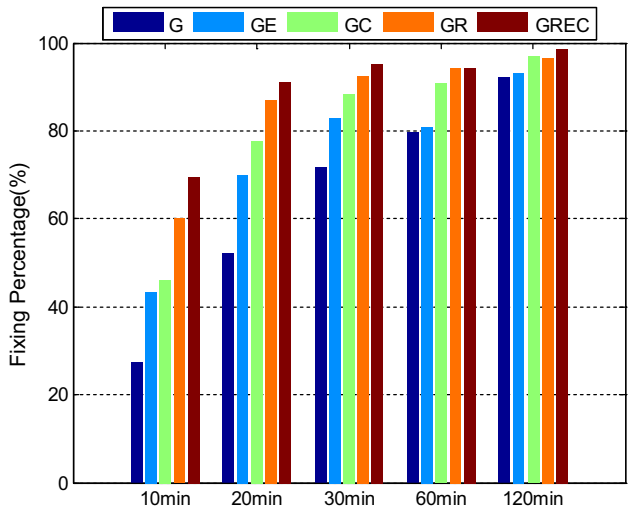

Fig. 16 Fixing percentage at different session lengths for single-,dual- and four-system kinematic PPP AR

IGSO satellites in the radial, cross and along directions can be improved by about 82.4, 47.3 and 49.6%, respectively, and the improvement in orbit accuracy for BDS MEO satellites in the three directions can reach about 50.5, 19.5 and 53.7%, respectively. Compared to the final precise orbit products (GBM) provided by GFZ, the averaged RMS values of QZSS satellites are 27.1, 39.7 and 43.7 cm in the radial, cross and along directions, respectively, over a period of 1 month. Our results also show that the real-time PCE solution can benefit from the proposed multi-GNSS POD strategy. Comparing with the post-processed final precise clock products, an accuracy of better than 6 cm is achievable for the GNSS real-time satellite clocks due to the hourly ultra-rapid orbit products.

Based on the multi-GNSS products, GCRE four-system kinematic precise point positioning can be performed to assess the contribution of multi-GNSS to PPP AR. The result indicates that, with the addition of the BDS, GLONASS and Galileo observations to the GPS-only processing, GCRE PPP AR solution presents the shortest average TTFF of 10.5 min under 7° cutoff elevation, while the TTFF of GPS-only, GR, GE and GC PPP AR solutions is 27.6, 14.7, 19.8 and 16.9 min, respectively. Multi-GNSS fixed solutions based on four-system data offer the shortest TTFF and highest accuracy under different cutoff elevations. When the cutoff elevation reaches 30°, TTFF of GPS-only, GR, GE and GC results is increased to 118.5, 49.4, 76.3 and 47.1 min, respectively, while TTFF of the GCRE fixed solutions is 18.6 min. Within 10 min observational data, the fixing percentage of GPS-only, GE, GC, GR is 27.3, 43.3, 46.1 and 60.1%, respectively. But with four-system, the fixing rate of multi-GNSS PPP AR results can be significantly improved to about 70.0%. Utilizing 20 min observational data, the fixing rate of GREC fixed solutions can even reach up to 91.2%. In summary, the results show that the fixing rate for PPP AR can be improved by introducing four-system combined observations. This is also due to the fact that the four-system solution provides more ambiguity candidates for partial AR compared to other solutions. In the future, we will further optimize the models and strategies for POD, including high-order ionospheric corrections, improving solar radiation pressure models, and so on. Therefore, a better performance of real-time PPP AR is expected to be achieved due to the real-time precise products with higher quality.

Acknowledgements Thanks go to the International GNSS Service (IGS) for providing multi-GNSS data and products. This study was financially supported by China Scholarship Council (CSC, File No. 201606270206) and the National Natural Science Foundation of China (Grant No. 41774030).

References

Beutler G, Brockmann E, Gurtner W, Hugentobler U, Mervart L, Rothacher M, Verdun A (1994) Extended orbit modeling techniques at the CODE processing center of the international GPS service for geodynamics (IGS): theory and initial results. Manuscr Geod 19:367–386

Cai C, Gao Y (2013) Modeling and assessment of combined GPS/GLONASS precise point positioning. GPS Solut 17:233–236

Dach R, Schaer S, Hugentobler U (2006) Combined multi-system GNSS analysis for time and frequency transfer. In: Proceedings of the European frequency and time forum, pp 530–537

El-Mowafy A, Deo M, Rizos C (2016) On biases in precise point positioning with multi-constellation and multi-frequency GNSS data. Meas Sci Technol 27(3):035102. https://doi.org/10.1088/0957-0233/27/3/035102

El-Mowafy A, Deo M, Kubo N (2017) Maintaining real-time precise point positioning during outages of orbit and clock corrections. GPS Solut 21(3):937–947

Ge M, Gendt G, Rothacher M, Shi C, Liu J (2008) Resolution of GPS carrier-phase ambiguities in precise point positioning with daily observations. J Geod 82(7):389–399

Ge M, Zhang H, Jia X, Song S, Wickert J (2012) What is achievable with the current COMPASS constellation? GPS World November, pp 29–34

Geng J, Shi C (2017) Rapid initialization of real-time PPP by resolving undifferenced GPS and GLONASS ambiguities simultaneously. J Geod 91(4):361–374

Hadas T, Bosy J (2015) IGS RTS precise orbits and clocks verification and quality degradation over time. GPS Solut 19(1):93–105

Jakowski N, Wilken V, Schlueter S, Stankov SM, Heise S (2005) Ionospheric space weather effects monitored by simultaneous ground and space based GNSS signals. J Atmos Sola Terr Phys 67(12):1074–1084

Kouba J (2009) A guide to using international GNSS service (IGS) products. http://igscb.jpl.nasa.gov/igscb/resource/pubs/UsingIGSProductsVer21.pdf. Accessed May 2009

Li X, Li X, Yuan Y, Zhang K, Zhang X, Wickert J (2017) Multi-GNSS phase delay estimation and PPP ambiguity resolution: GPS, BDS, GLONASS, Galileo. J Geod 1–30. https://doi.org/10.1007/s00190-017-1081-3

Li X, Ge M, Zhang H, Wickert J (2013) A method for improving uncalibrated phase delay estimation and ambiguity-fixing in real-time precise point positioning. J Geod 87(5):405–416

Li X, Ge M, Dai X, Ren X, Fritsche M, Wickert J, Schuh H (2015) Accuracy and reliability of multi-GNSS real-time precise positioning: GPS, GLONASS, BeiDou, and Galileo. J Geod 89(6):607–635

Liu J, Ge M (2003) PANDA software and its preliminary result of positioning and orbit determination. Wuhan Univ J Nat Sci 8:603–609

Montenbruck O, Hauschild A, Steigenberger P, Hugentobler U, Teunissen P, Nakamura S (2013) Initial assessment of the COMPASS/BeiDou-2 regional navigation satellite system. GPS Solut 17(2):211–222

Montenbruck O, Steigenberger P, Prange L, Deng Z, Zhao Q, Perosanz F, Romero I, Noll C, Stürze A, Weber G, Schmid R, MacLeod K, Schaer S (2017) The multi-GNSS experiment (MGEX) of the international GNSS service (IGS)—achievements, prospects and challenges. Adv Sp Res 59:1671–1697

Prange L, Orliac E, Dach R, Arnold D, Beutler G, Schaer S, Jäggi A (2017) CODE's five-system orbit and clock solution—the challenges of multi-GNSS data analysis. J Geod 91:345

Schaer S, Beutler G, Rothacher M, Brockmann E, Wiger A, Wild U (1999) The impact of the atmosphere and other systematic errors on permanent GPS networks. In: Proceedings of president IAG symposium on positioning, Birmingham, UK, 19–24 July 1999, p 406

Schaffrin B, Bock Y (1988) A unified scheme for processing GPS dual-band phase observations. Bull Geod 62:142–160

Steigenberger P, Hugentobler U, Montenbruck O, Hauschild A (2011) Precise orbit determination of GIOVE-B based on the CONGO network. J Geod 85:357–365

Shi C, Zhao Q, Hu Z (2013) Precise relative positioning using real tracking data from COMPASS GEO and IGSO satellites. GPS Solut 17(1):103–119

Teunissen P, Odolinski R, Odijk D (2014) Instantaneous BeiDou+GPS RTK positioning with high cut-off elevation angles. J Geod 88(4):335–350. https://doi.org/10.1007/s00190-013-0686-4

Wang F, Chen X, Guo F (2015) GPS/GLONASS combined precise point positioning with receiver clock modeling. Sensors 15(7):15478–15493

Zhang X, Li X, Guo F (2011) Satellite clock estimation at 1 Hz for realtime kinematic PPP applications. GPS Solut 15(4):315–324. https://doi.org/10.1007/s10291-010-0191-7

Zhang X, Wu M, Liu W, Li X, Yu S, Lu C, Wickert J (2017) Initial assessment of the COMPASS/BeiDou-3: new-generation navigation signals. J Geod 91(10):1225–1240

Zumberge J, Heflin M, Jefferson D, Watkins M, Webb F (1997) Precise point positioning for the efficient and robust analysis of GPS data from large networks. J Geophys Res 102(B3):5005–5017. https://doi.org/10.1029/96JB03860